Voltage Sensorless Improved Model Predictive Direct Power Control for Three-Phase Grid-Connected Converters

Amir Masoud Bozorgi[1], Hosein Gholami-Khesht[2], Mehdi Farasat[1], Shahab Mehraeen[1], Mohammad Monfared[2]
[1] Division of Electrical and Computer Engineering, Louisiana State University, Baton Rouge, LA, USA
[2] Department of Electrical and Computer Engineering, Ferdowsi University of Mashhad, Mashhad, Iran

***Abstract*—Despite distinctive advantages such as fast dynamic, simple concept and ease of implementation, model predictive direct power control (MPDPC) suffers from some major drawbacks. First, in order to provide sinusoidal currents and low-ripple powers, very high sampling rates are required for MPDPC implementation. Furthermore, this method requires accurate knowledge of system parameters and its performance deteriorates in presence of parameter uncertainties. In this paper, an improved MPDPC is proposed, which features: 1) high current and power quality at low sampling frequencies, 2) less sensitivity to parameter uncertainties, particularly unknown grid inductance, and 3) voltage sensorless operation. The first and second features are achieved by incorporating the concept of switching duty cycles into the conventional MPDPC. In the proposed method, two voltage vectors are applied during a control period and their duty cycles are obtained by a fuzzy logic modulator. The proposed fuzzy logic modulator works based on the real and reactive power errors. Eventually, voltage sensorless operation is accomplished by designing a full-order observer. Thanks to voltage sensorless operation, the system volume and cost can be reduced. Through extensive hardware-in-the-loop tests, the superiority of the proposed MPDPC in comparison with two conventional MPDPCs is demonstrated.**

Keywords— Model predictive direct power control (MPDPC), fuzzy logic modulator, full-order observer.

I. INTRODUCTION

Model predictive direct power control (MPDPC) is recently being employed in renewable energy based distributed power generation systems owning to its simple concept and fast dynamics in controlling the power flow [1]-[5]. In this method, all possible switching states of a power converter are evaluated in each sampling period and the state that minimizes a predefined cost function is chosen and then applied to the converter during the next control period. Since in each sampling period the converter switching state is determined directly based on the cost function evaluation, MPDPC does not require a modulator. Consequently, the switching frequency of a converter controlled by MPDPC is variable and the produced currents contain a widespread spectrum of harmonics [3].

In [6]-[11], in order to reduce the current distortion as well as the power ripple, MPDPC techniques with constant switching frequency (CS-MPDPC) are presented where in each sampling period, three voltage vectors (a zero and two active voltage vectors) are chosen and applied. Normally, these vectors are chosen based on the position of the grid voltage vector and to calculate the optimum duty ratio of each voltage vector , the least square optimization method is used. In [10], it is concluded that, in some load conditions, selection of the voltage vectors based on the sector of the grid voltage vector results in negative duty cycles of the active voltage vectors; hence, the negative duty cycles should be equated with zero under these conditions. This issue leads to periodic fluctuations in the generated real and reactive powers and also, low order harmonic content in the currents. Accordingly, new methods to select active voltage vectors and to avoid negative duty cycles are proposed in [9]-[11]. Although these methods, which employ three voltage vectors in each control period, cause reduced power ripple and current distortion, they, however, are highly sophisticated and less efficient because of increased average switching frequency.

In order to address this issue, improved MPDPC strategies based on the concept of duty cycle control (D-MPDPC) are proposed in [12]-[14]. In these methods, an active and a zero voltage vector are selected and applied in each period. This idea is valid if applying zero voltage vectors did not affect the real and reactive powers; however, as it is discussed in [1], although zero voltage vectors do not have considerable effect on the reactive power, they result in reduction of real power. Therefore, using any active voltage vector along with a zero voltage vector results in steady-state error in real power control. Furthermore, applying zero voltage vector following the active voltage vector, as proposed in [12]-[14], leads to lose of control over the output voltage phase angle. In order to overcome this drawback and improve the flexibility of power control, either active or zero voltage vectors are suggested to be considered as the second vector in [13]. Despite improvements in current and power quality, the control method suffers from high complexity, computational burden, and average switching frequency.

Another problematic feature of model predictive methods is their dependency on accurate knowledge of system parameters. This problem is intensified in D-MPDPC techniques, such as the ones in [12] and [13], since the system model is utilized for power prediction, optimal voltage vector selection, duty cycle optimization, and compensation of digital implementation delay, and as a result, they are sensitive to system uncertainties, such as grid and filter inductance variations.

In this paper, an improved D-MPDPC is proposed which addresses the shortcomings of previously discussed MPDPC techniques. The proposed method is comprised of three main

Research described in this paper was supported by Louisiana Board of Regents' grant no. 2015-18-RD-A-04.

building blocks: predictive power controller, fuzzy logic modulator and a full order observer. In the proposed method, only two switching vectors are employed in each sampling period in order to achieve low current distortion, power ripple and average switching frequency. The errors between the predicted and reference real and reactive powers are fed to the fuzzy logic modulator as the inputs, and the duty cycles of voltage vectors are obtained as the outputs. Duty cycles determined by the fuzzy modulator are used for power prediction and based on the MPDPC theory, optimal voltage vectors are selected. As a result, the accuracy of calculated duty cycles does not depend on knowledge of system model and its parameters. The full-order observer is used to compensate the digital implementation delay, estimate grid voltages and realize sensorless operation, and ameliorate robustness of the proposed MPDPC against system parameter uncertainties.

II. System Equations and Model

The topology of a grid-connected PWM converter, including a voltage source, two-level inverter with an L-type output filter, is depicted in Fig. 1. In this figure, v_{gabc}, i_{abc} and v_{abc} are three-phase grid voltages, three-phase currents and the converter output voltages, respectively. Also, v_{PCC} is voltage at the point of common coupling (PCC). In addition, L_g, L_f and r_f denote grid inductance and filter inductance and its equivalent series resistance, respectively.

The system three-phase voltage equations can be decoupled into two independent equations in stationary reference frame by using the space vector theory as follows

$$v_{\alpha\beta} = v_{g\alpha\beta} + r_f i_{\alpha\beta} + L\frac{di_{\alpha\beta}}{dt} \tag{1}$$

where, $i_{\alpha\beta}$, $v_{g\alpha\beta}$ and $v_{\alpha\beta}$ are α-β components of grid current, grid voltage and converter ac output voltage in stationary reference frame, respectively, and $L=L_f+L_g$. In practice, accurate value of L_g is unknown and therefore, an estimated value is considered in (1).

Assuming sinusoidal and balance grid voltages, α-β components of the grid voltage, $v_{g\alpha}$ and $v_{g\beta}$, can be expressed as

$$\begin{cases} v_{g\alpha} = V_m \sin(\omega t) \\ v_{g\beta} = -V_m \cos(\omega t) \end{cases} \tag{2}$$

Here, V_m represents the grid phase voltage amplitude and ω is the grid angular frequency. Taking derivative from (2), instantaneous variations of grid voltage components can be obtained as

$$\begin{cases} \dfrac{dv_{g\alpha}}{dt} = \omega V_m \cos(\omega t) = -\omega v_{g\beta} \\ \dfrac{dv_{g\beta}}{dt} = \omega V_m \sin(\omega t) = \omega v_{g\alpha} \end{cases} \tag{3}$$

Based on (1) and (3), state-space equation of the system can be written as

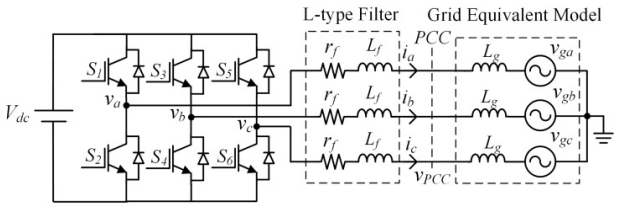

Fig.1. Topology of grid connected PWM converter

$$\frac{dx(t)}{dt} = Ax(t) + Bu(t) \tag{4}$$

where, $x = \left[i_{\alpha\beta}(t), v_{g\alpha\beta}(t)\right]^T$, $A = \begin{bmatrix} \frac{-r_f}{L} I & -\frac{1}{L} J \\ O & \omega J \end{bmatrix}$, $B = \begin{bmatrix} \frac{1}{L} I \\ O \end{bmatrix}$ and $u(t) = \left[v_{\alpha\beta}(t)\right]^T$ are state variables vector, state matrix , input matrix and input vector respectively. In addition, $I = \begin{bmatrix} 1 & 0 \\ 0 & 1 \end{bmatrix}$, $O = \begin{bmatrix} 0 & 0 \\ 0 & 0 \end{bmatrix}$ and $J = \begin{bmatrix} 0 & -1 \\ 1 & 0 \end{bmatrix}$.

Discrete equivalent of (4) can be written as

$$\begin{cases} x(k+1) = A_d x(k) + B_d u(k) \\ A_d = L^{-1}[(\mathrm{s}I - A)^{-1}] \approx I + AT_S \\ B_d = \int_0^{T_S} A_d(T_S - \tau) B d\tau \approx BT_S \end{cases} \tag{5}$$

In (5), T_s is sampling time, s is Laplace operator and L^{-1} is inverse Laplace transform.

Due to digital implementation delay, a sample delay must be considered, and hence (5) is rewritten as

$$x(k+1) = A_d x(k) + B_d u(k-1) \tag{6}$$

Apparent power injected to the grid at the $(k+1)th$ sample can be calculated by [18]

$$S(k+1) = v_{g\alpha\beta}(k+1) \times i^*_{\alpha\beta}(k+1) \tag{7}$$

where, "*" denotes complex conjugate. Substituting (6) into (7) and after some simplifications, apparent power equation can be derived as

$$\begin{aligned} S(k+1) = (1 + j\omega T_S)[(1 - r_f \frac{T_S}{L}) S(k) + \\ \frac{T_S}{L} v^*_{\alpha\beta}(k-1) v_{g\alpha\beta}(k) - \frac{T_S}{L} \left| v_{g\alpha\beta}(k) \right|^2] \end{aligned} \tag{8}$$

III. Full-Order Observer Design

In order to fully compensate digital implementation delay, a full-order observer is employed in the proposed MPDPC. The observer helps with compensating digital implementation delay by predicting the state variables in the $(k+2)th$ sample, rather than the $(k+1)th$ sample, realizing a two-step MPDPC. Moreover, observer facilitates voltage sensorless operation of the PWM converter, which in turn can reduce converter size and cost and enhance reliability. The observer equation can be obtained by adding a feedback term, which is the error

between measured and estimated outputs, to the state space equation of system in (6)

$$\begin{cases} \hat{x}(k+1) = A_d\hat{x}(k) + B_d u(k-1) + G(y(k) - \hat{y}(k)) \\ \hat{y} = C_d\hat{x}(k),\ C_d = \begin{bmatrix} I & O \\ O & O \end{bmatrix} \end{cases} \tag{9}$$

Here, y and $\hat{y}$ are measured and estimated outputs, respectively, $\hat{x}$ is estimated state variables and G is the observer gain. The observer gain is chosen such that the dynamic of estimation error is asymptotically stable [15]. The dynamic error equation can be defined as

$$\begin{cases} e(k+1) = A_O e(k) \\ e(k+1) = x(k+1) - \hat{x}(k+1) \\ A_O = A_d - GC_d \end{cases} \tag{10}$$

In this equation, if the observer gain (G) is selected in a way that eigenvalues of matrix A_O lie in unity circle, the dynamic of error equation would be asymptotically stable [15]. In other words, regardless of its initial value, $e(0)$, estimation error approaches zero ($e(k+1) \to 0$) or estimation states approaches real values ($\hat{x}(k+1) = x(k+1)$). In order to satisfy the abovementioned conditions, the observer gain can be obtained by solving the following equation

$$G = \begin{bmatrix} g_1 & -g_2 & g_3 & -g_4 \\ g_2 & g_1 & g_4 & g_3 \end{bmatrix}^T \tag{11}$$

$$\left|\lambda I - A_O\right| = \left|\lambda I - A_d + GC_d\right| = (\lambda - \lambda_1)^2(\lambda - \lambda_2)^2$$

where, λ_1 and λ_2 are desired eigenvalues of dynamic errors. Components of matrix G can be then calculated as follows

$$\begin{cases} g_1 = 2 - \dfrac{r_f T_S}{L} - \lambda_1 - \lambda_2 \\ g_2 = -\omega T_S \\ g_3 = -\dfrac{L}{T_S}(1 + \lambda_1\lambda_2 - \lambda_1 - \lambda_2 - \omega^2 {T_S}^2) \\ g_4 = L\omega(2 - \lambda_1 - \lambda_2) \end{cases} \tag{12}$$

IV. Proposed Predictive Direct Power Control

Fig. 2 illustrates the block diagram of the proposed method. As the first step, measured currents at the kth sample are fed into the observer to estimate voltages and currents in the (k+1)th sample. Next, estimated real and reactive powers at the (k+1)th sample are calculated using the estimated voltages and currents. The estimated powers are then compared with their corresponding reference values and the errors are fed to the fuzzy logic modulator. Therefore, fuzzy inputs are as follows

$$\begin{cases} Input\,1: \Delta P = P_{ref} - \hat{P}(k+1) \\ Input\,2: \Delta Q = Q_{ref} - \hat{Q}(k+1) \end{cases} \tag{13}$$

The fuzzy logic modulator role is to determine the duty cycle of applied voltage vectors. The fuzzy logic is based on Mamdani fuzzy inference system [16], [17]. The input and output membership functions used in the designed fuzzy logic modulator are shown in Fig. 3.

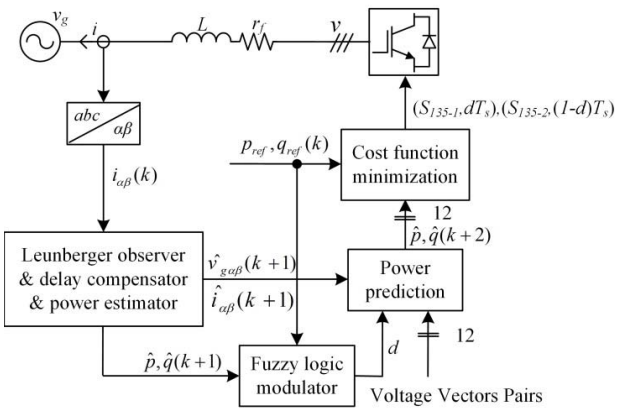

Fig. 2. Block diagram of the proposed MPDPC with fuzzy-based modulator and reduced number of sensors

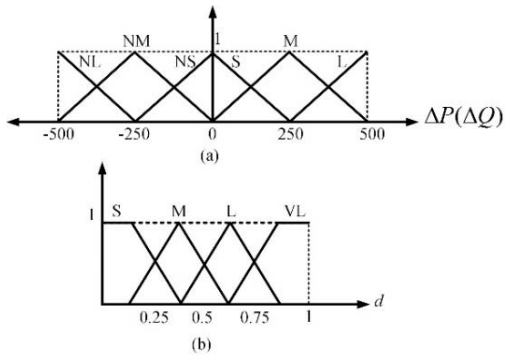

Fig. 3. Membership function of (a) inputs, and (b) output of fuzzy modulator

By examining Fig. 4, one can see that variation of real power around grid voltage vector position axis is not symmetrical. Therefore, separate membership functions for positive and negative fuzzy inputs must be defined. Table I summarizes the fuzzy logic rules. It is worth noting that the fuzzy modulator output is duty cycle of the first voltage vector. After obtaining the duty cycles, the switching states for the next sample are determined by using the equation for apparent power prediction. Assuming voltage vectors v_{ref1} and v_{ref2} are selected as the first (main) and second vector with duty cycles of d and 1-d, respectively, the apparent power at t=(k+1+d)T_s and t=(k+2)T_s is predicted as (14) and (15), respectively

$$\hat{S}(k+1+d) = (1 + j\omega dT_S)[(1 - \frac{r_f dT_S}{L})\hat{S}(k+1) + \frac{dT_S}{L} v^*_{ref\,1,\alpha\beta}(k)\hat{v}_{g\alpha\beta}(k+1) - \frac{dT_S}{L}\left|\hat{v}_{g\alpha\beta}(k+1)\right|^2] \tag{14}$$

$$\hat{S}(k+2) = (1 + j\omega(1-d)T_S)[(1 - \frac{r_f(1-d)T_S}{L})\hat{S}(k+1+d) + \frac{(1-d)T_S}{L} v^*_{ref\,2,\alpha\beta}(k)\hat{v}_{g\alpha\beta}(k+1+d) - \frac{(1-d)T_S}{L}\left|\hat{v}_{g\alpha\beta}(k+1+d)\right|^2] \tag{15}$$

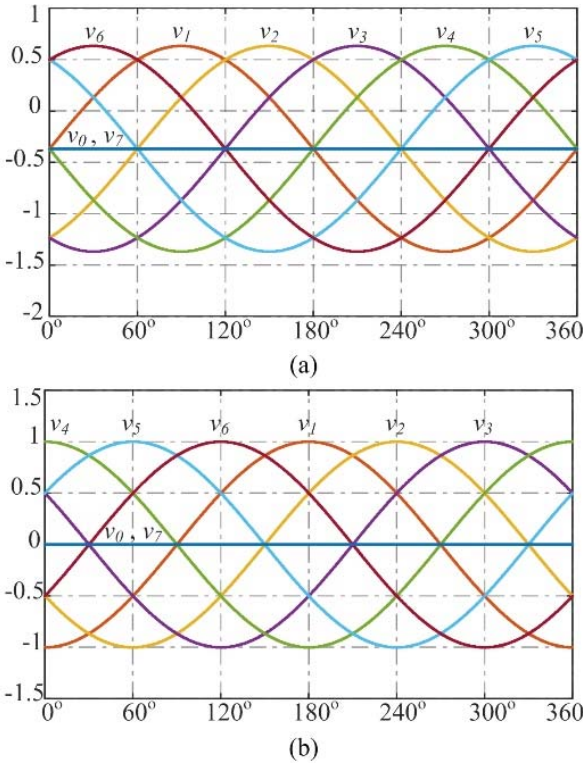

Fig. 4. Instantaneous (a) real, and (b) reactive power variations versus grid voltage vector position.

TABLE I
FUZZY RULES

		Reactive Power Error					
		NL	NM	NS	S	M	L
Active Power Error	NL	VL	L	L	M	L	VL
	NM	L	M	S	M	M	L
	NS	VL	L	M	M	L	VL
	S	VL	L	L	S	S	L
	M	L	L	L	S	L	L
	L	VL	L	L	VL	L	VL

Although different control objectives can be included in the cost function, the following cost function is employed in this paper

$$J = \left(S_{ref}(k) - \hat{S}(k+2) \right)^2 \tag{16}$$

Here, S_{ref} represents the apparent power reference value.

The predicted apparent power from (15), i.e. $\hat{S}(k+2)$, is used in (16) and the pair of voltage vectors that minimize the cost function are selected. It is noteworthy to mention that different combinations of voltage vector pairs can be examined for determining the optimal pair. In order to reduce the computational burden, twelve different voltage vector pairs are examined in the proposed method. The first six pairs are comprised of one active voltage vectors along with one zero voltage vector, i.e. (V_1, V_0), (V_2, V_7),…, (V_5, V_0), (V_6, V_7). The remaining six pairs are comprised of two consecutive active voltage vectors, i.e. (V_1, V_2), (V_2, V_3),…, (V_5, V_6), (V_6, V_1). The considered selection of consecutive voltage vectors ensures minimum number of changes in the switches states, hence reduced average switching frequency, as well.

TABLE II
HARDWARE-IN-THE-LOOP RESULTS

Method	THD [%]	P_{ripple} [w]	Q_{ripple} [var]
Conventional MPDPC [3]	7.69	224	206
D-MPDPC [12]	5.57	165	172
Proposed D-MPDPC	4.89	143	135

V. RESULTS AND DISCUSSION

The performance of three methods, including conventional MPDPC [3], D-MPDPC [12] and the proposed MPDPC, is investigated through hardware-in-the-loop (HIL) studies. The HIL setup consists of an OP4510 real-time simulator from Opal-RT Technologies Inc. operating with Kintex7 FPGA and a TI TMS320F28335 DSP. In the first test, steady-state performance of three methods is compared when reference of real and reactive powers of the grid-connected converter is set at 5 kW and 0 kVar, respectively. The obtained results are depicted in Figs. 5 to 7. Although D-MPDPC shows a rather acceptable performance, it can be observed from the real power waveform that there is a negative shift in the generated real power due to the use of only zero vectors as the second voltage vector. The obtained average switching frequency for D-MPDPC in [12] and the proposed MPDPC is approximately 20 kHz and 16.2 kHz, respectively. As summarized in Table II, the proposed method outperforms the other two methods in term of current quality and power ripple.

In the second test, the dynamic performance of three methods is evaluated through step changes in real and reactive powers. Figs. 8, 9 and 10 show the dynamic performance of the converter under conventional MPDPC [3], D-MPDPC [12] and the proposed MPDPC, respectively. As it can be seen, the proposed method has fast dynamic as two other conventional MPDPC methods. Robustness of the proposed method against system parameter uncertainties is verified by introducing a 0.5 mH error in the grid inductance. As illustrated in Fig. 11, performance of the proposed method is not degraded and acceptable results are obtained.

VI. CONCLUSION

A simple and effective fuzzy logic-based method for calculating switching duty cycles of model predictive direct power controlled grid-connected converters is proposed. In contrast to the existing methods, which use the power prediction model for calculation of duty cycles, the duty cycles are obtained based on the real and reactive power errors. In addition, a full-order observer is adopted, which allows compensation of digital implementation delay, eliminating grid voltage sensors and offers robustness against system parameter uncertainties.

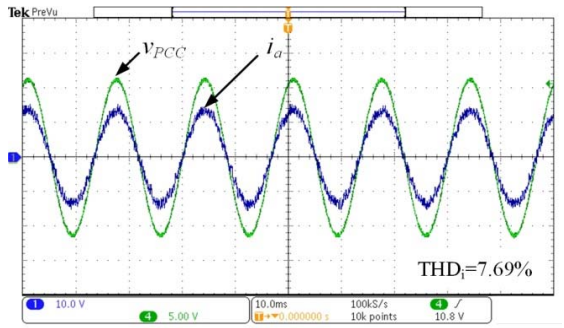

(a)

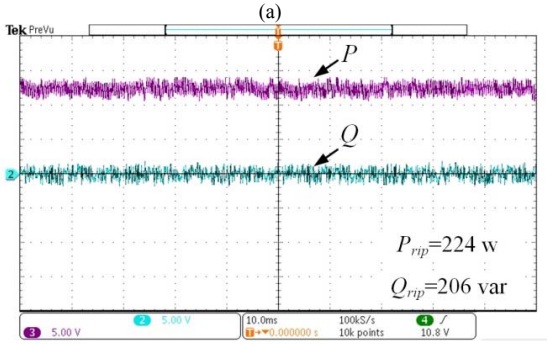

(b)

Fig. 5. HIL steady state results under conventional MPDPC [3], waveforms of (a) the grid voltage and current (b) injected real and reactive powers (v_{PCC}: 75 V/div, i_a: 14 A/div, P_{rip}: 2000 w/div, Q_{rip}: 2000 var/div, time:10ms/div).

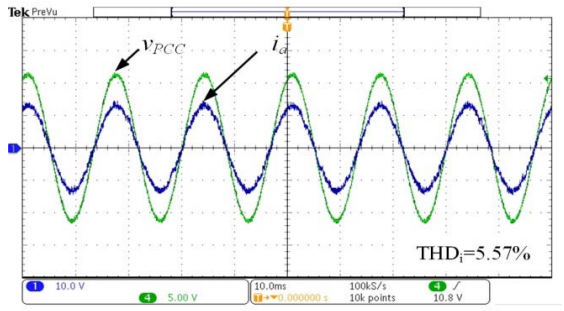

(a)

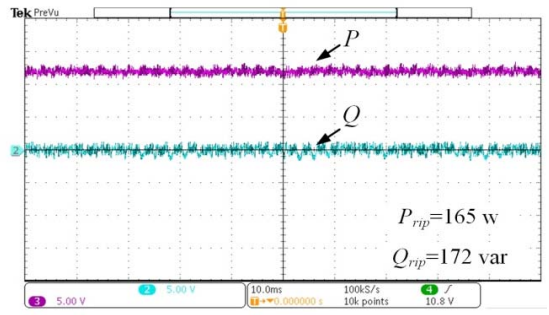

(b)

Fig. 6. HIL steady state results under D-MPDPC [12], waveforms of (a) the grid voltage and current (b) injected real and reactive powers (v_{PCC}: 75 V/div, i_a: 14 A/div, P_{rip}: 2000 w/div, Q_{rip}: 2000 var/div, time:10ms/div).

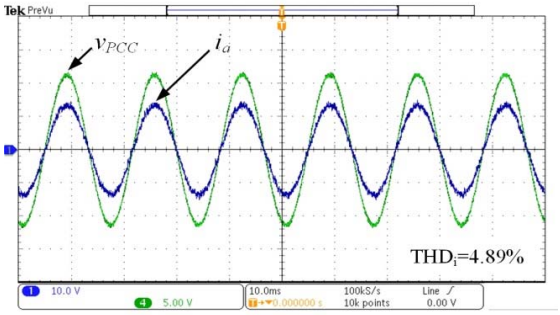

(a)

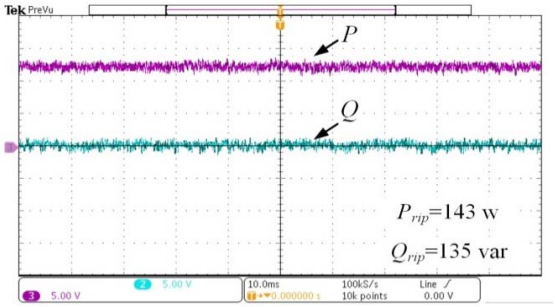

(b)

Fig. 7. HIL steady state results under proposed MPDPC, waveforms of (a) the grid voltage and current (b) injected real and reactive powers (v_{PCC}: 75 V/div, i_a: 14 A/div, P_{rip}: 2000 w/div, Q_{rip}: 2000 var/div, time:10ms/div).

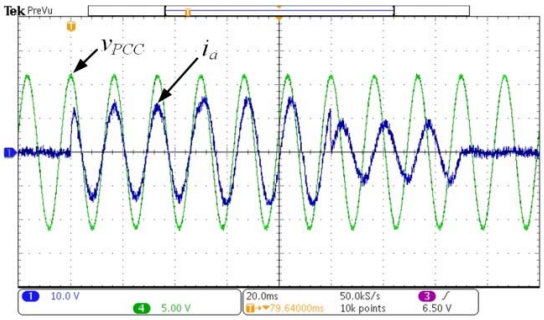

(a)

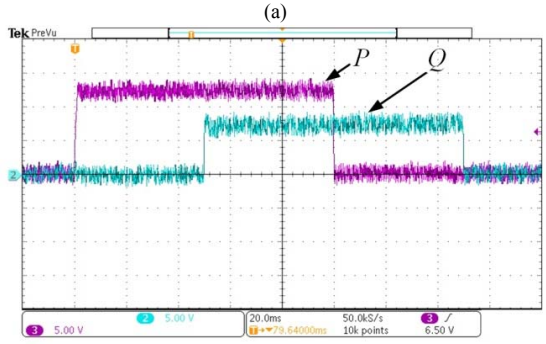

(b)

Fig. 8. HIL results for dynamic performance of conventional MPDPC [3], waveforms of (a) the grid voltage and current (b) injected real and reactive powers (v_{PCC}: 75 V/div, i_a: 14 A/div, P_{rip}: 2000 w/div, Q_{rip}: 2000 var/div, time:20ms/div).

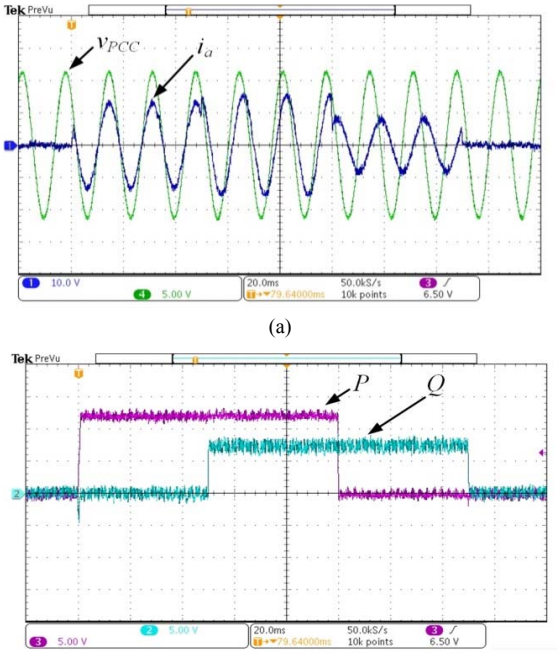

Fig. 9. HIL results for dynamic performance of D-MPDPC [12], waveforms of (a) the grid voltage and current (b) injected real and reactive powers (v_{PCC}: 75 V/div, i_a: 14 A/div, P_{rip}: 2000 w/div, Q_{rip}: 2000 var/div, time:20ms/div).

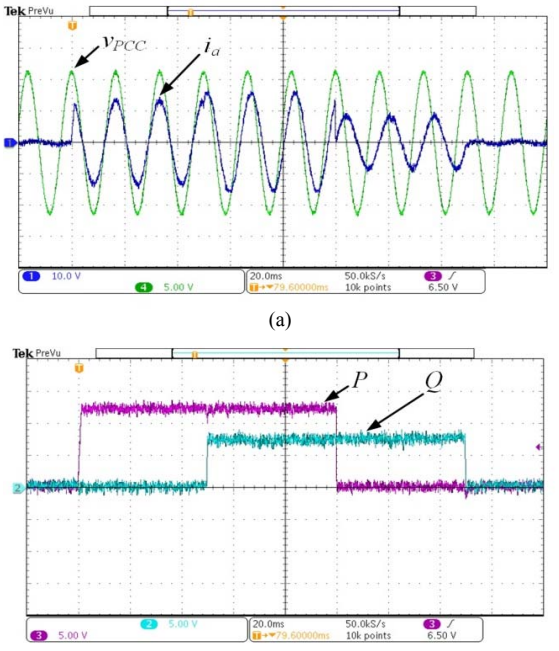

Fig. 10. HIL results for dynamic performance of proposed MPDPC, waveforms of (a) the grid voltage and current (b) injected real and reactive powers (v_{PCC}: 75 V/div, i_a: 14 A/div, P_{rip}: 2000 w/div, Q_{rip}: 2000 var/div, time:20ms/div).

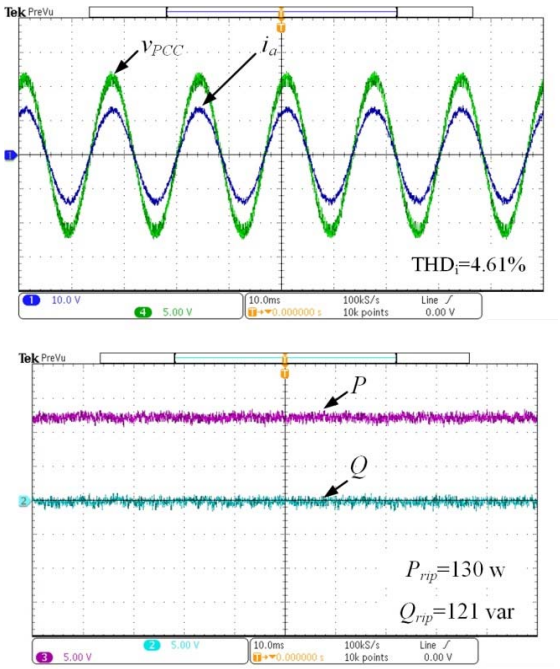

Fig.11. HIL results for steady state waveforms of the grid voltage and current and injected real and reactive powers under the proposed MPDPC with 0.5mH error in grid inductance (v_{PCC}: 75 V/div, i_a: 14 A/div, P_{rip}: 2000 w/div, Q_{rip}: 2000 var/div, time:10ms/div).

REFERENCES

[1] S. Vazquez, A. Marquez, R. Aguilera, D. Quevedo, J. I. Leon, and L. G. Franquelo, "Predictive optimal switching sequence direct power control for grid-connected power converters," *IEEE Trans. Ind. Electron.*, vol. 62, no. 4, pp. 2010–2020, 2015.

[2] D. E. Quevedo, R. P. Aguilera, M. A. Perez, P. Cortes, and R. Lizana, "Model predictive control of an AFE rectifier with dynamic references," *IEEE Trans. Power Electron.*, vol. 27, no. 7, pp. 3128–3136, Jul. 2012.

[3] P. Cortes, J. RodrÍguez, P. Antoniewicz, and M. Kazmierkowski, "Direct power control of an AFE using predictive control," *IEEE Trans. Power Electron.*, vol. 23, no. 5, pp. 2516–2523, Sep. 2008.

[4] E. Afshari, G. R. Moradi, Y. Yang, B. Farhangi and S. Farhangi, "A review on current reference calculation of three-phase grid-connected PV converters under grid faults," *2017 IEEE Power and Energy Conference at Illinois (PECI)*, Champaign, IL, 2017, pp. 1-7.

[5] J. Hu, J. Zhu, and D. G. Dorrell, "Model-predictive control of grid-connected inverters for PV systems with flexible power regulation and switching frequency reduction," in *2013 IEEE Energy Conversion Congress and Exposition*, 2013, vol. 51, no. 1, pp. 540–546.

[6] X. Wang and D. Sun, "Three-vector based Low-complexity model predictive direct power control strategy for doubly fed induction generator," *IEEE Trans. Power Electron.*, vol. 32, no. 1, pp. 773-782, Jan. 2017.

[7] P. Antoniewicz and M. P. Kazmierkowski, "Virtual-flux-based predictive direct power control of AC/DC converters with online inductance estimation," *IEEE Trans. Ind. Electron.*, vol. 55, no. 12, pp. 4381–4390, Dec. 2008.

[8] S. A. Larrinaga, S. Member, M. Angel, and R. Vidal, "Predictive Control Strategy for DC / AC Converters Based on Direct Power Control," *IEEE Trans. Ind. Electron.*, vol. 54, no. 3, pp. 1261–1271, 2007.

[9] J. Hu, "Improved Deadbeat predictive DPC strategy of grid-connected DC–AC converters with switching Loss minimization and delay compensations," *IEEE Trans. Ind. Informatics*, vol. 9, no. 2, pp. 728–738, May 2013.

[10] J. Hu and Z. Q. Zhu, "Improved voltage-vector sequences on Deadbeat predictive direct power control of reversible three-phase grid-connected voltage-source converters," *IEEE Trans. Power Electron.*, vol. 28, no. 1, pp. 254–267, Jan. 2013.
[11] Z. Song, W. Chen, and C. Xia, "Predictive direct power control for three-phase grid-connected converters without sector information and voltage vector selection," *IEEE Trans. Power Electron.*, vol. 29, no. 10, pp. 5518–5531, 2014.
[12] Y. Zhang, W. Xie, Z. Li, and Y. Zhang, "Model predictive direct power control of a PWM rectifier with duty cycle optimization," *IEEE Trans. Power Electron.*, vol. 28, no. 11, pp. 5343–5351, Nov. 2013.
[13] Z. Zhang, X. Feng, H. Fang, and R. Kennel, "Ripple-reduced model predictive direct power control for active front-end power converters with extended switching vectors and time-optimised control," *IET Power Electron.*, vol. 9, no. 9, pp. 1914–1923, Jul. 2016.
[14] X. Wang and D. Sun, "Three-vector based Low-complexity model predictive direct power control strategy for doubly fed induction generator," *IEEE Trans. Power Electron.*, vol. 32, no. 1, pp. 773-782, Jan. 2017.
[15] H. Gholami-Khesht and M. Monfared, "Deadbeat direct power control for grid connected inverters using a full-order observer," in *Proc. 4th International Conference on Electric Power and Energy Conversion Systems (EPECS)*, pp. 1–5, 2015.
[16] A. M. Bozorgi, M. Farasat, S. Jafarishiadeh, "Model Predictive Current Control of Surface-Mounted Permanent Magnet Synchronous Motor with Low Torque and Current Ripple," *IET Power Electron.*, available online , April 2017.
[17] A. Bozorgi, M. Farasat, and S. Jafarishiadeh, "Improved model predictive current control of permanent magnet synchronous machines with fuzzy based duty cycle control," in Proc. *Energy Conversion Congress and Exposition (ECCE)*, pp. 1-6, 2016.
[18] E. Afshari, B. Farhangi, Y. Yang and S. Farhangi, "A low-voltage ride-through control strategy for three-phase grid-connected PV systems," *2017 IEEE Power and Energy Conference at Illinois (PECI)*, Champaign, IL, 2017, pp. 1-6.